

Evolution of the H₂O and OH Maser Emission in W75 N

P. Colom¹, E. E. Lekht^{2*}, M. I. Pashchenko², G. M. Rudnitskii², and A. M. Tolmachev³

¹*LESIA, Observatoire de Paris-Meudon, CNRS, UPMC, Université Paris-Diderot, 92195 Meudon Cedex, France*

²*Lomonosov Moscow State University, Sternberg Astronomical Institute, Moscow, 119992 Russia*

³*Pushchino Radio Astronomy Observatory, Astro Space Center, Lebedev Physical Institute, Russian Academy of Sciences, Pushchino, Moscow oblast, 142290 Russia*

Received December 14, 2017; in final form, January 26, 2018

Abstract—The results of a study of H₂O and OH maser emission in the complex region of active star formation W75 N are presented. Observations were obtained using the 22-m radio telescope of the Pushchino Radio Astronomy Observatory (Russia) and the Nançay radio telescope (France). Flaring H₂O maser features may be identified with maser spots associated with the sources VLA 1 and VLA 2. The main H₂O flares occurred in VLA 1. The flare emission was associated with either maser clusters having closely spaced radial velocities and sizes up to ~ 2 AU or individual features. The maser emission is generated in a medium where turbulence on various scales is present. Analysis of the line shapes during flare maxima does not indicate the presence of the simplest structures—homogeneous maser condensations. Strong variability of the OH maser emission was observed. Zeeman splitting of the 1665-MHz line was detected for several features of the same cluster at a radial velocity of +5.5 km/s. The mean line-of-sight magnetic field in this cluster is ~ 0.5 mG, directed away from the observer. Flares of the OH masers may be due to gas compression at a shock or MHD wave front.

DOI: 10.1134/S1063772918060045

1. INTRODUCTION

The source W75 N is located in the composite molecular complex Cygnus-X, where the active star formation is ongoing. The estimated distance to the object is 2 kpc. W75 N hosts the ultracompact H II regions VLA 1, VLA 2, and VLA 3 [1], strong IR sources [2], and clusters of H₂O, OH, and methanol maser features [3, 4]. The three VLA sources are considered to be objects at different evolutionary stages.

VLA 1 is identified with a radio jet. This continuum source spans 2000 AU in the northeast–southwest direction. H₂O masers are located along the jet. According to VLBI maps of this source, the H₂O masers form three groups: A, B, and C. Group A is located toward the center of the continuum source (a protostellar object), while groups B and C are located to the southwest of this source. Only groups B and C were detected as a result of subsequent observations performed in 2012 [5].

The radio continuum source VLA 2 has not been resolved spatially ($\leq 0.08''$). This source is associated with a protoplanetary disk. The mass of the central star is $\approx 10 M_{\odot}$, and the radius of the system is about 160 AU. There is an expanding circumstellar

envelope with a complex hierarchical structure, which hosts individual maser features, maser clusters, inhomogeneous filaments and multilink chains, separate arcs (shell fragments), and other complex forms (see, e.g., [6, 7]).

W75 N is a unique source, because maps of H₂O maser features for this object have been obtained for many epochs, starting from 1992.86. These maps made it possible to reveal hierarchical structures in the VLA 1 jet and VLA 2 disk and to trace their evolution, as well as to determine the proper motions of maser features. However, Lekht et al. [7, 8] did not find strong motions of individual clusters of maser spots relative to the central sources in VLA 1 and VLA 2. They suggest that the maser activity could be due to the passage of a strong magnetohydrodynamical (MHD) wave that excites maser emission in corresponding zones of low mobility of the maser source.

The OH masers in W75 N are concentrated in two activity centers, associated with radio continuum sources, namely, the compact H II regions VLA 1 and VLA 2. The OH emission in W75 N is highly variable [9–11].

Interferometric observations of the OH masers in W75 N have been performed in a number of studies

*E-mail: lekht@sai.msu.ru

(see, e.g. [12–16]). The OH maser condensations visible in a VLBA map of W75 N for July 1, 1998 [14] form an elongated arc around VLA 1. This structure is consistent with a circumstellar disk model. Pairs of spatially coincident emission features (maser spots) with opposite senses of circular polarization were detected in the main lines at 1665 and 1667 MHz. These pairs can be used to measure the radial magnetic fields.

A strong magnetic field was detected in W75 N during a powerful flare of the OH maser emission [16]. W75 N maps in the OH line at 1667 MHz from VLBA data obtained in 2001 [16] show a number of Zeeman pairs, which were used to determine the magnetic field, which proved to be as strong as 40 mG. Fish et al. [13] detected proper motions of maser spots in the main OH lines with a mean velocity of +3.5 km/s, comparable to the velocity of thermal turbulence, in both VLA 1 and VLA 2.

Long-term monitoring of W75 N has been used to trace the evolution of separate flares of the H₂O maser emission, which occur in this source fairly often (see, e.g. [17, 18]).

2. OBSERVATIONS AND ANALYSIS

Monitoring of W75 N at 1.35 cm has been carried out with the 22-m radio telescope of the Pushchino Radio Astronomy Observatory since the end of 1979. We present here spectra obtained in 2015–2017. The antenna gain was 25 Jy/K for a point source of unpolarized emission. The noise temperature varied in the range 130–230 K, depending on the weather conditions. The spectrum analyzer was a 2048-channel autocorrelator with a spectral resolution of 6.1 kHz (0.0822 km/s for the 1.35-cm line). Results for observations carried out before 2015 were published earlier [17, 18]. The full catalog of H₂O spectra obtained as a result of our monitoring of W75 N spans the interval 1980–2017.

Our present study is based on our monitoring of W75 N during 2015–2017, as well as on some data obtained in 2011–2014. The mean time interval between successive observations was about 1.2 months.

Monitoring of the OH lines at 18 cm was carried out in 2007–2016 using the Nanzay radio telescope (France). The 18-cm main beamwidth at a declination of $\delta = 0^\circ$ is $3.5' \times 19'$ in right ascension and declination, respectively. The telescope gain for $\lambda = 18$ cm and $\delta = 0^\circ$ is 1.4 K/Jy. The noise temperature of the liquid-helium-cooled amplifiers varied in the range 35–60 K, depending on the observing conditions. The spectrum analyzer was a 8192-channel autocorrelator split into several sections, each yielding an independent spectrum in one of the two main

OH lines (1665 and 1667 MHz) in one of four polarizations. In our observations, the spectrum analyzer was split into eight 1024-channel sections. In the observations of all four OH lines, the analyzer was split into 16 512-channel sections. For the main lines, the frequency resolution was 763 Hz (0.0686 km/s) and the full bandwidth was 35 km/s (from –9 to 26 km/s).

Figures 1–5 show the spectra of the H₂O maser emission. Due to the large range of the flux densities, the individual figure scales are different. Emission features overlapping those in the previous spectra are drawn by dotted lines. The epochs of the observations are indicated. The double vertical arrows show the scales for the vertical axes in Jansky. The horizontal axes plot the radial velocities relative to the Local Standard of Rest (LSR). A wide range of velocities was observed, from –74 to 92 km/s. The right panels in Figs. 1–5 show the central parts of the maser spectra.

Figure 6 shows the radial-velocity and flux-density variations of the main emission features. The radial-velocity variations were fitted by straight lines (dashed). Features with closely spaced velocities probably form clusters; for convenience, we have called them configurations and numbered them. The associations of the configurations with VLA 1 or VLA 2 is indicated. Strong variability was observed, in particular, small jumps in the radial velocity. A careful analysis showed that we observed the sequential appearance of features with close radial velocities. We tested the robustness of the detections of the velocity jumps using reference features in the spectra; this eliminated random errors in the observations. The jumps hinder identification of the emission features with specific maser spots. We can only associate the inferred configurations with previously detected clusters of maser spots.

The line widths at the flare maxima are indicated for most of the flares. The peaks of the emission are shown by arrows. The deviations of the data points from the fitted lines are significantly larger than the velocity uncertainties, and are related to real evolution of the maser emission. The epoch of the VLA observations (2012.54) is shown by the vertical line near the horizontal axis in the upper panel.

Figure 7 is the same as Fig. 6 for $V_{\text{LSR}} < 4$ km/s. The structures of the spectra in this velocity region are fairly simple. Here, fitting of the velocity variations is not necessary, since the velocity drifts of most of the emission features are clearly visible. Each feature is denoted by its own symbol.

The spectra of the main OH lines at 1665 and 1667 MHz in right- and left-circular polarization are shown in Figs. 8 and 9, by the bold and thin curves,

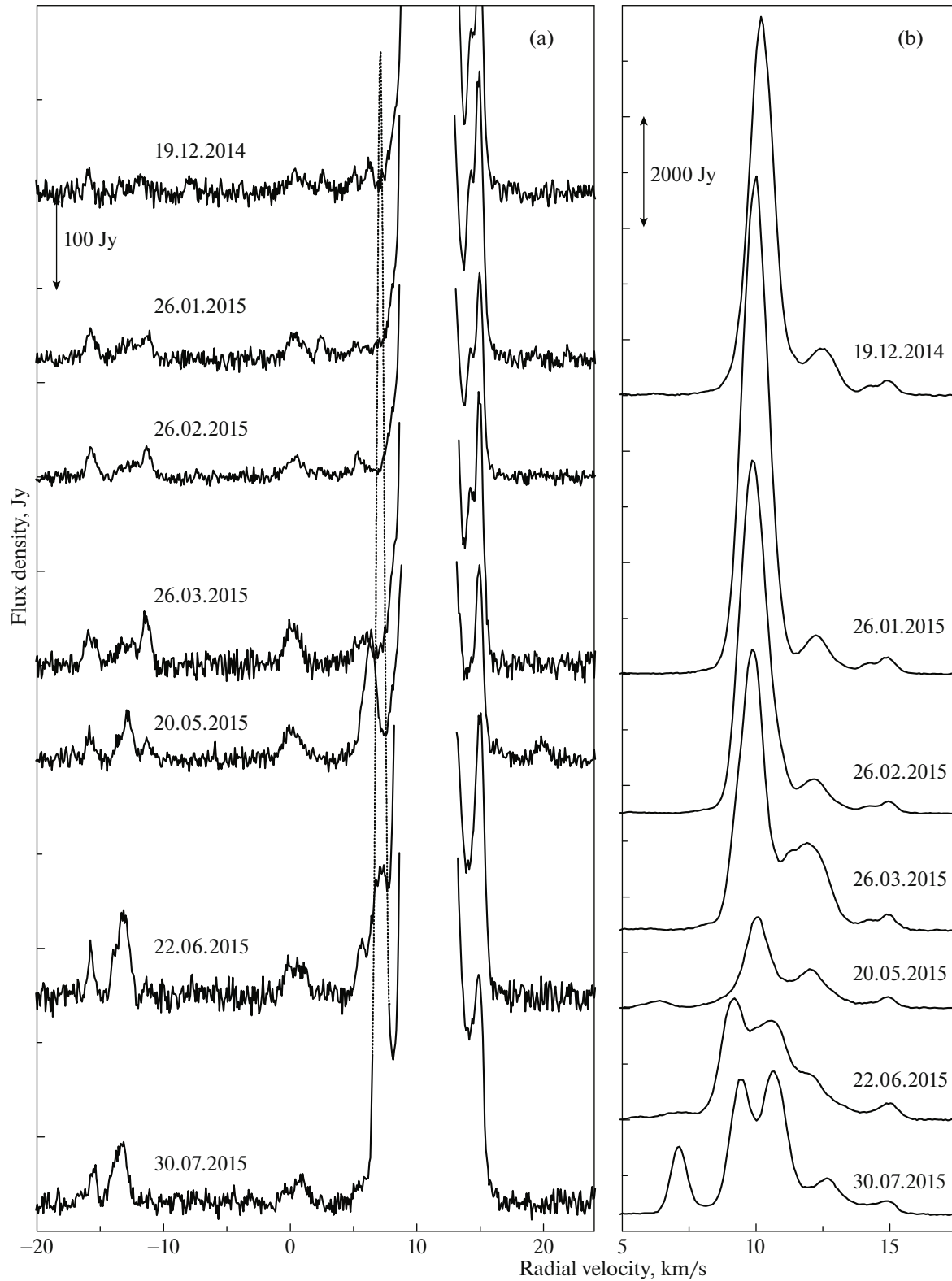


Fig. 1. Spectra of H₂O maser emission in W75 N (a) and their central parts (b) from December 2014 to June 2015. The double vertical arrows show the vertical scales.

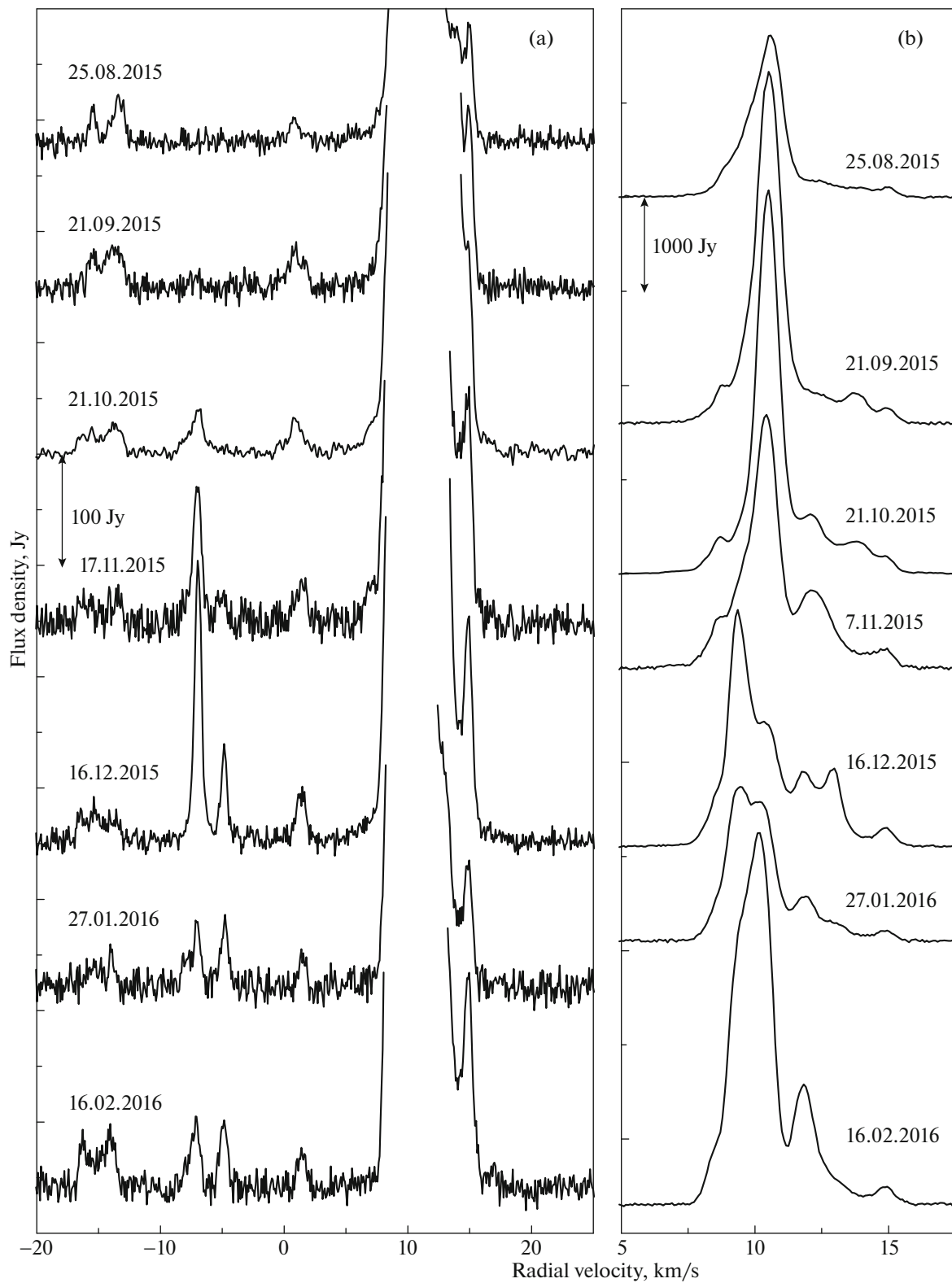


Fig. 2. Same as Fig. 1 for August 2015 to February 2016.

respectively. Spectra are shown only for radial velocities from -7 to $+16$ km/s, since we observed only sporadic weak emission features with flux densities

at 1667 MHz below 0.3 Jy outside this range. Two of these observed on August 8, 2013 at 21.8 and

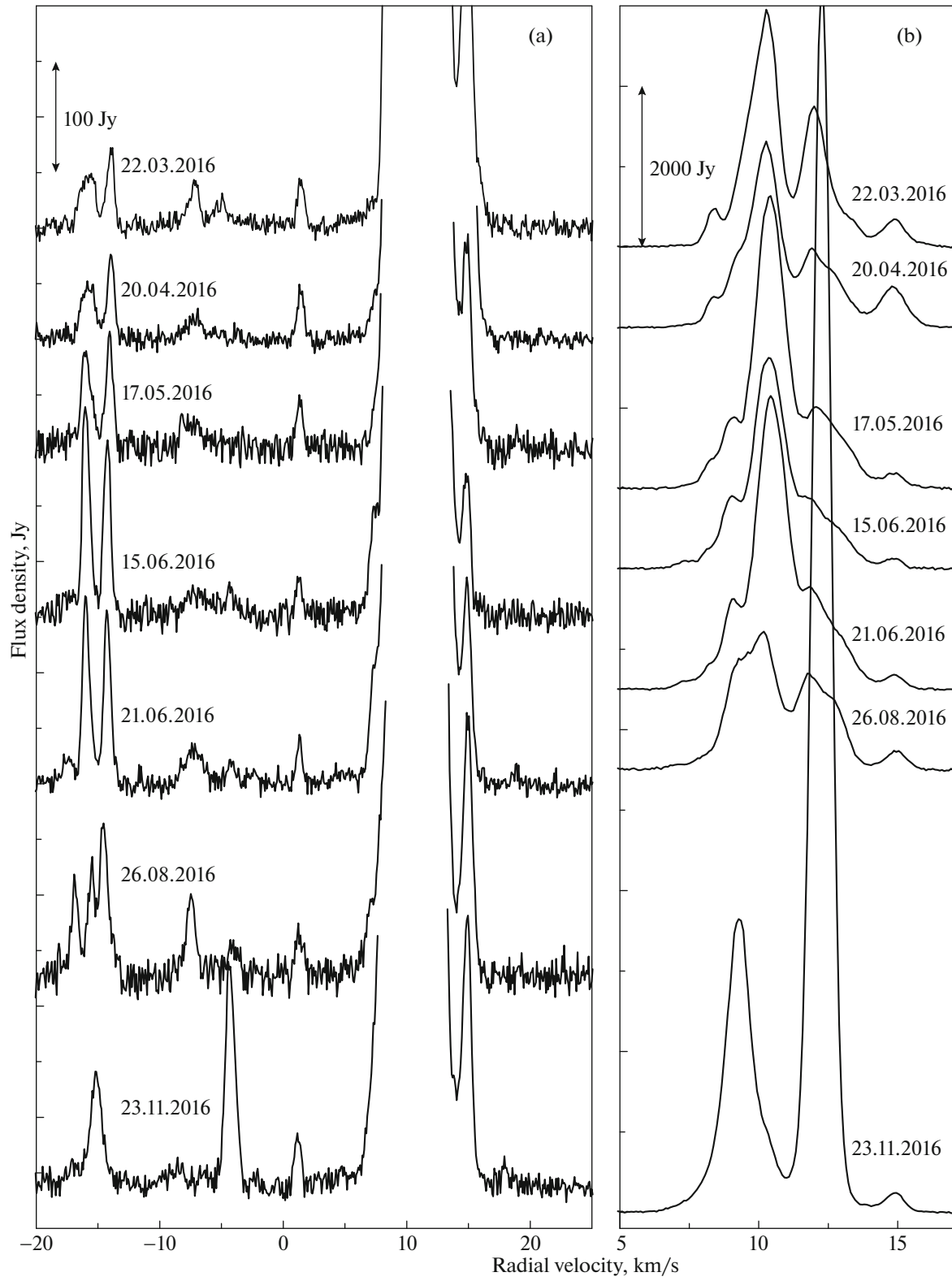


Fig. 3. Same as Fig. 1 for March–November 2016.

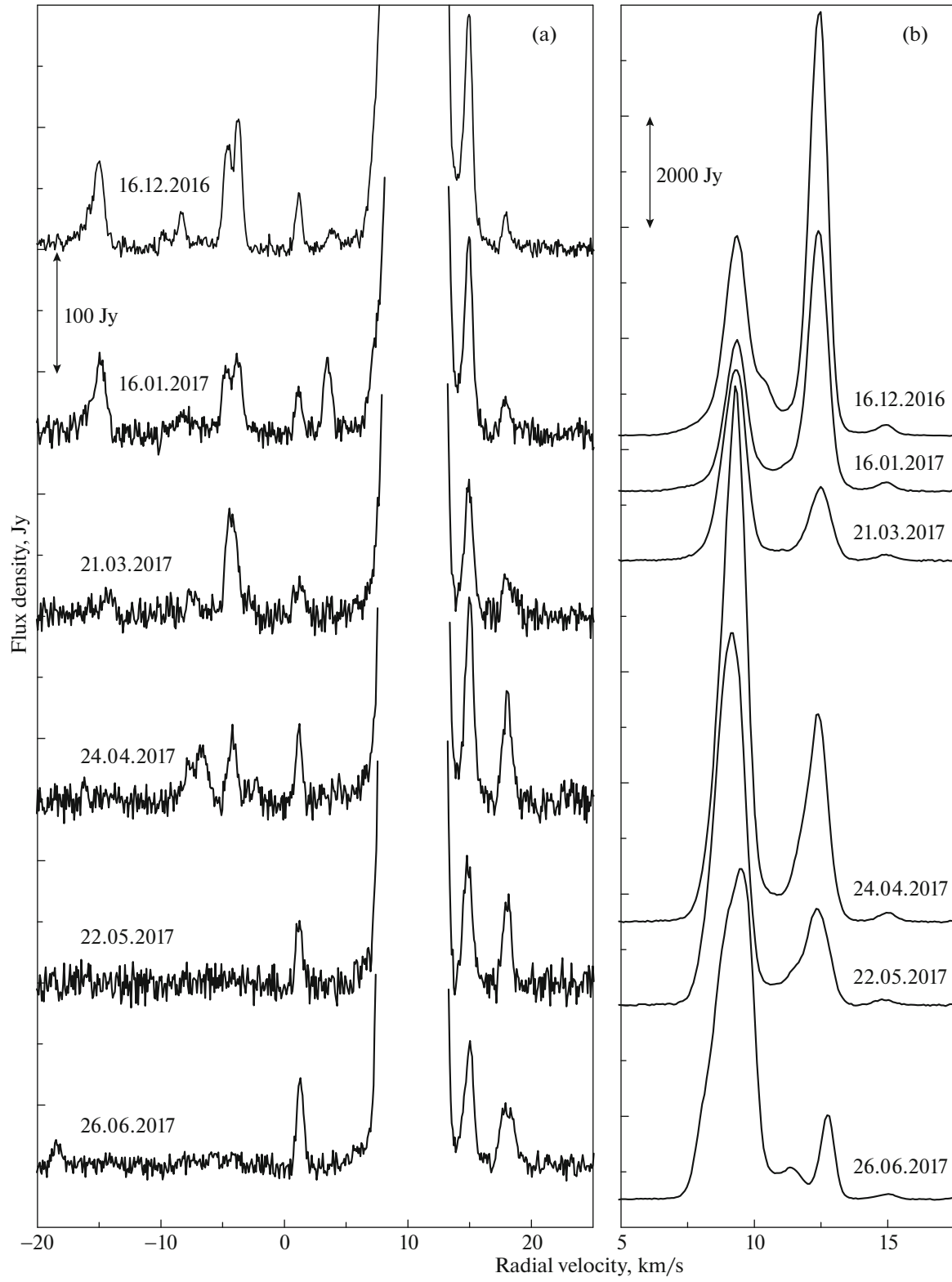


Fig. 4. Same as Fig. 1 for December 2016 to June 2017.

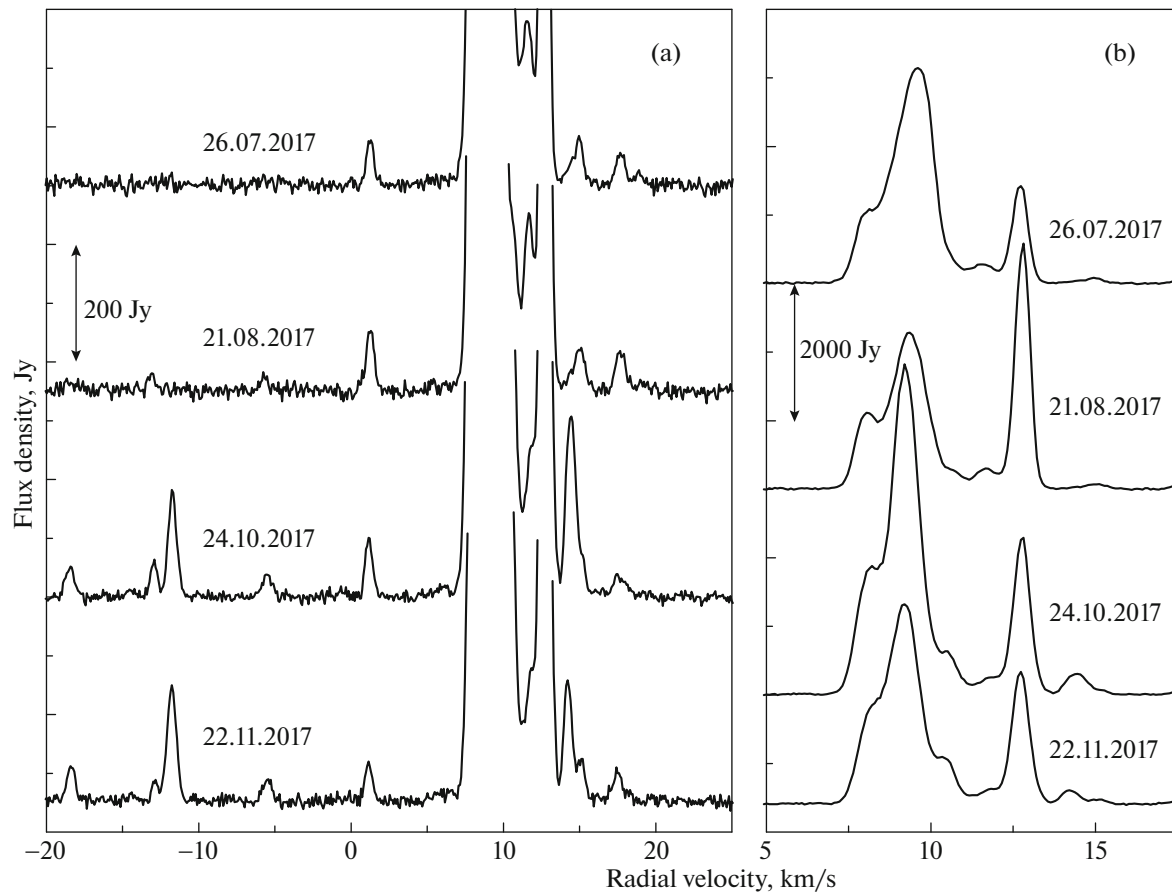


Fig. 5. Same as Fig. 1 for July–November 2017.

24.3 km/s coincide in velocity with two Zeeman pairs presented in [16].

Two spectral features near 5.5 km/s in right-circular polarization at 1665 MHz are marked 1 and 2. Note that, in the region of radial velocities shown, the spectra in both circular polarizations are similar and have complex structures, but slightly shifted in velocity. This shift appears as a result of Zeeman splitting in the magnetic field present in this region. No fewer than three features are present in this part of the spectrum, two being the strongest.

Figure 10 shows the radial-velocity variations for two features at 1665 MHz in both circular polarizations and the value of the radial magnetic field. The radial-velocity variations were fitted using a second-order polynomial. We did not use the Stokes parameter V , defined as the difference between the right- and left-circularly polarized fluxes, to determine the Zeeman splitting. When the splitting is very small and comparable to the line width, the Zeeman components are superimposed in velocity and the standard calculation of Stokes V leads to incorrect results.

Thus, we distinguished individual features for the right- and left-circular polarizations, determined their

radial velocities, fitted polynomials, and then used these polynomials to determine the velocity differences (Zeeman splitting), and found the corresponding radial magnetic fields. The curves for both features nearly coincide.

3. DISCUSSION

We detected water H_2O maser emission in a wide range of radial velocities (from -20 to $+20$ km/s), and fairly strong and continuously observable OH emission in a narrower range, from -6 to 16 km/s.

3.1. Identification and H_2O Variability of Individual Features

Our monitoring demonstrated that the strongest H_2O flares since 2006 occurred at radial velocities of 9.5–11.5 km/s. Analysis of maps for three epochs and our monitoring data showed that these flares are associated with VLA 1 (group B).

The H_2O maser activity in W75 N has remained very high beginning from the second half of 2012. Our first task was to discover which of the two sources was

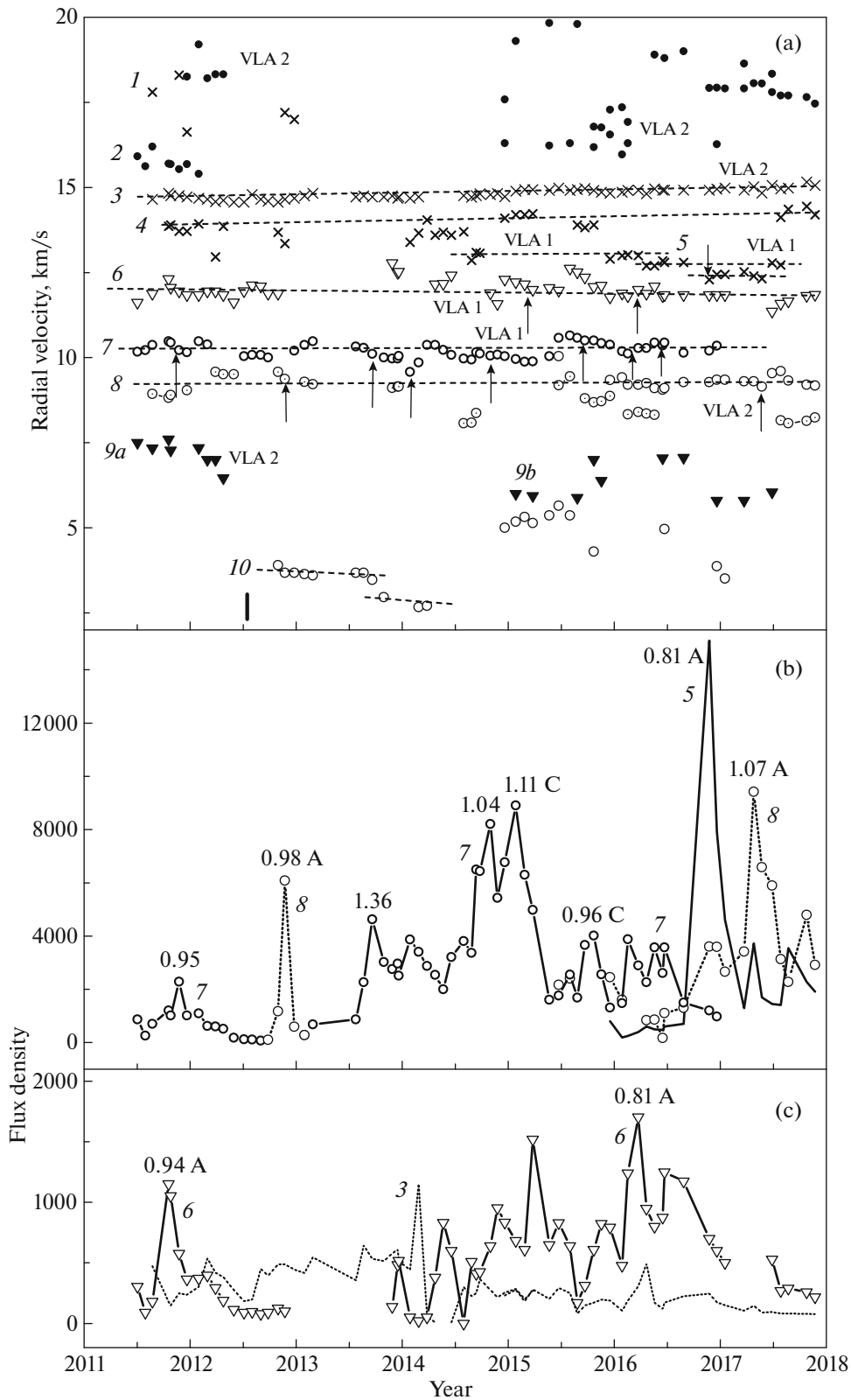


Fig. 6. Variability of the (a) radial velocity and (b, c) flux density of the main H₂O maser features at radial velocities 2–20 km/s. The features are numbered for convenience. Fits to the radial-velocity variations are shown by the dashed lines. The arrows show the positions of the emission maxima. The line width during the flare maximum is indicated for each flare.

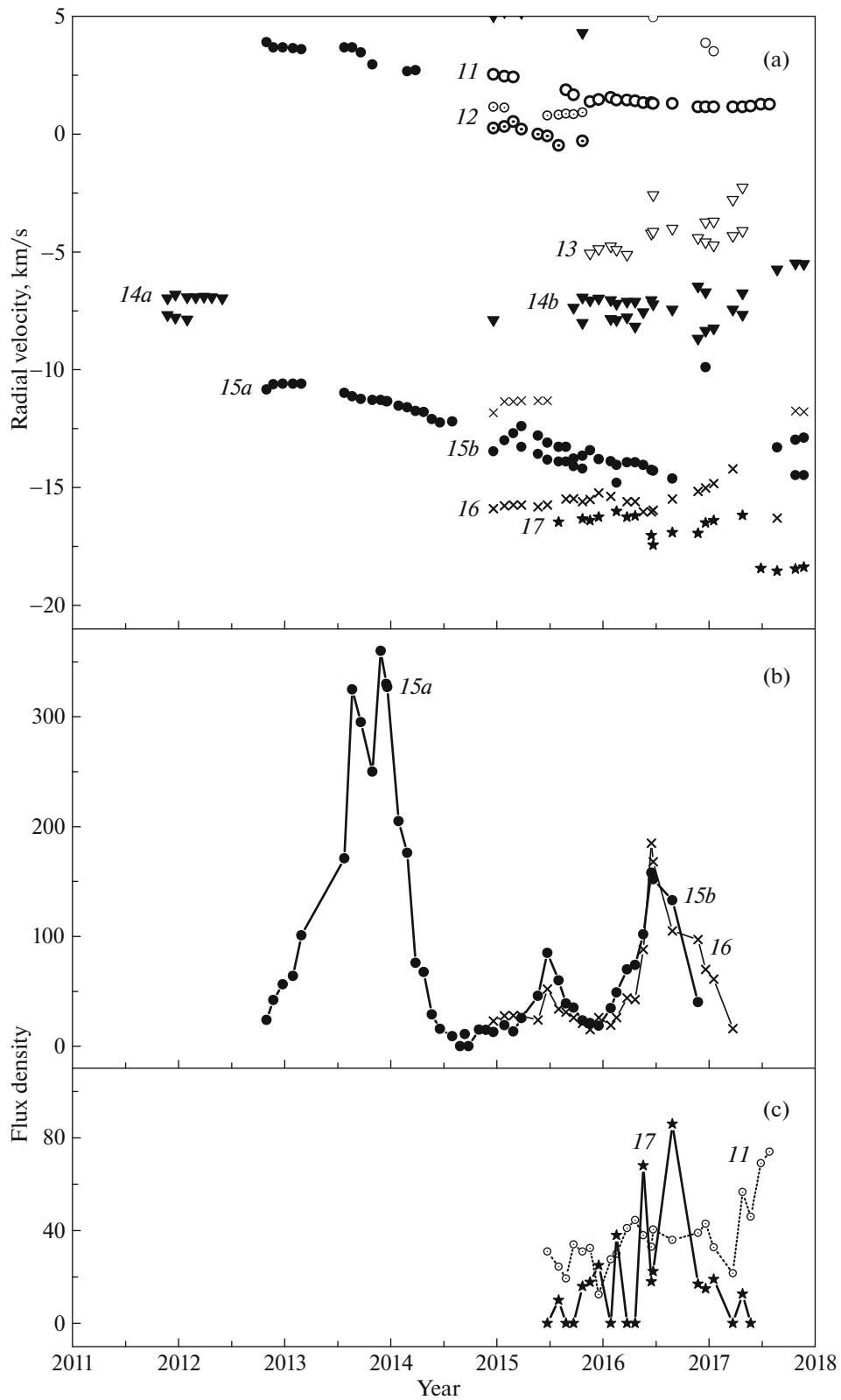


Fig. 7. Same as Fig. 6 for velocities from -21 to $+5$ km/s.

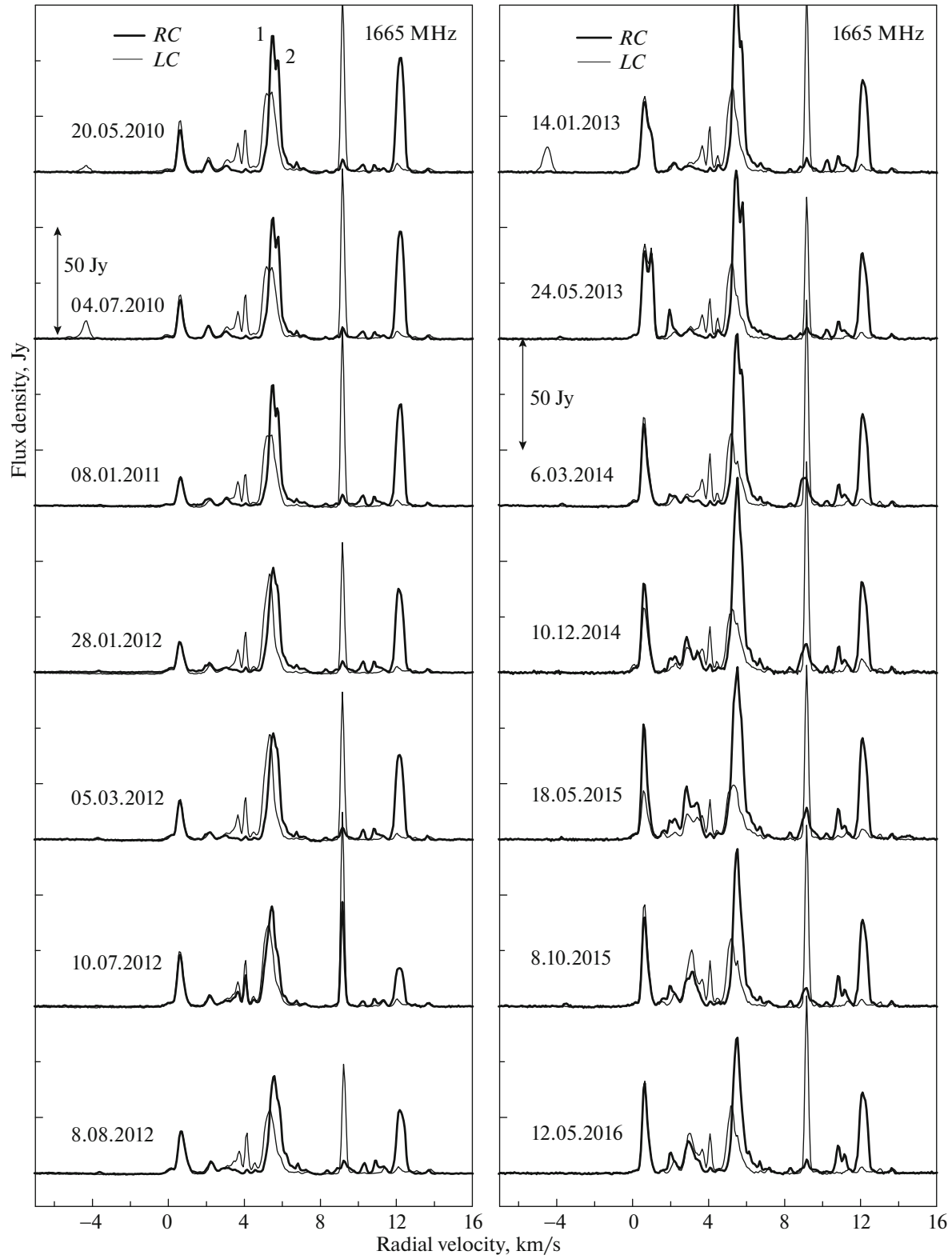


Fig. 8. Spectra of the OH maser emission at 1665 MHz.

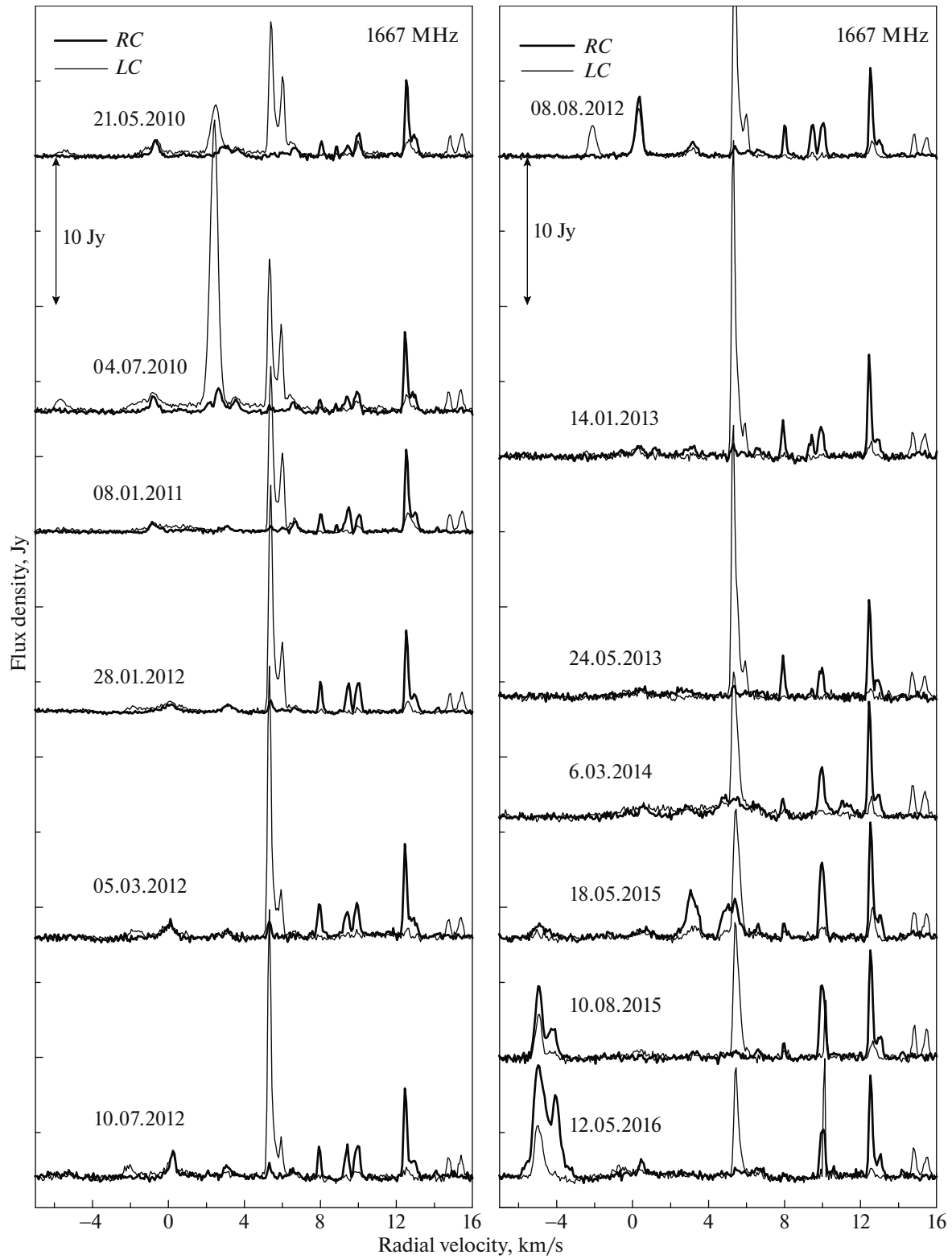


Fig. 9. Spectra of the OH maser emission at 1667 MHz.

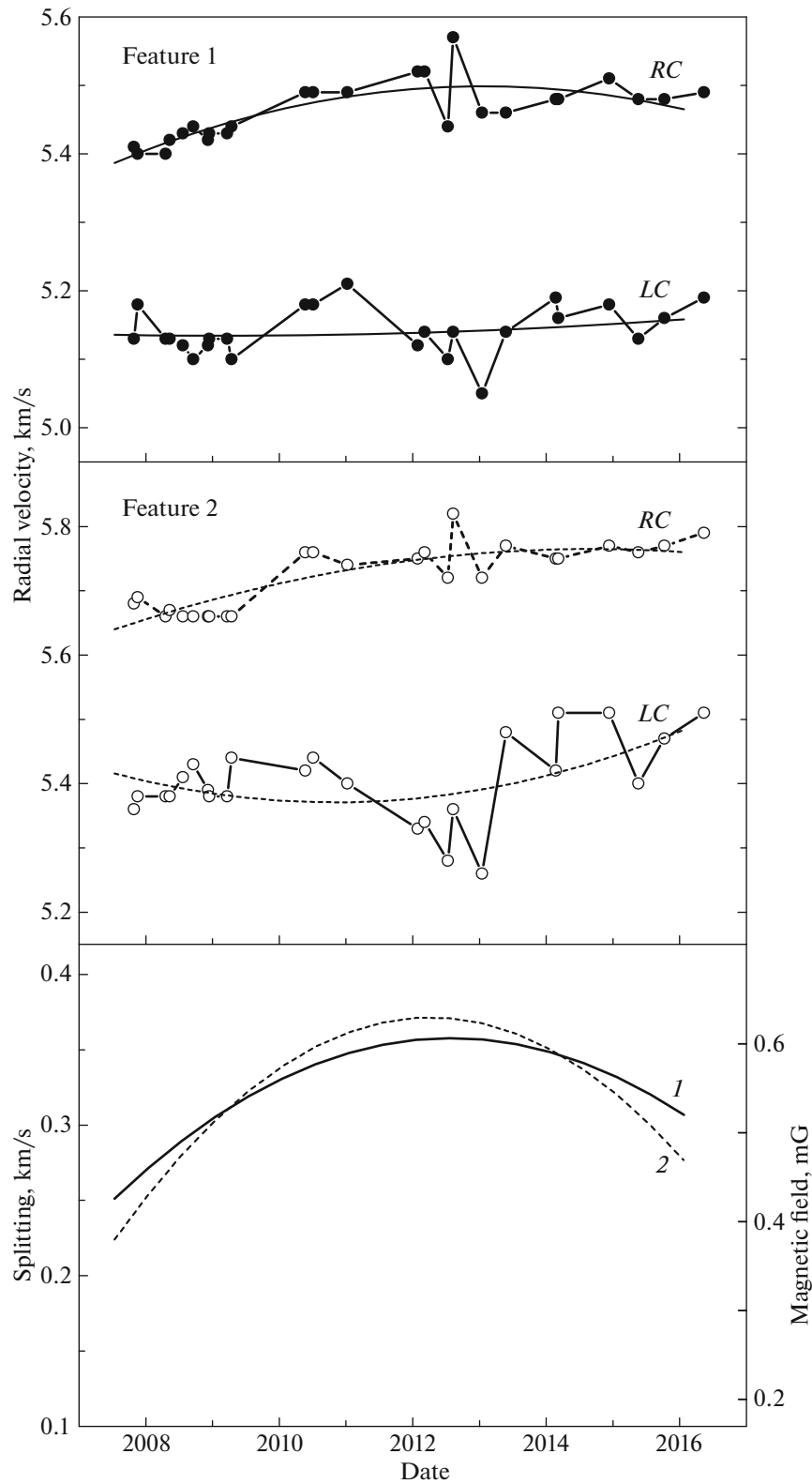


Fig. 10. Radial-velocity variations of two features at 1665 MHz for both circular polarizations and of the inferred line-of-sight magnetic field. The radial-velocity variations were fitted using second-order polynomials (see the text).

responsible for the observed activity. We tried to identify groups of features (configurations in Fig. 6) using VLBA observations. The latest results of such observations, for epoch 2012.54, were published in [5]. We also used data from [6–8].

The main configurations with strong emission are the structures 5, 6, and 7. These are reliably identified with maser clusters in VLA 1. It is impossible to identify them with specific spots due to their rapid evolution. The strongest emission, including a series of powerful flares, was observed in configuration 7, but only before 2017.

An emission feature at 6.8 km/s (see Fig. 6) observed in 2012–2013 [7] and from 2015 to the present is associated with a maser cluster in VLA 2 (a Keplerian disk). Emission at velocities of 1.5–3.5 km/s observed in 2005–2006 [7] and 2012–2013 is associated with this same source. No emission in this range is mentioned in [19, 20], and was probably absent at the epochs of those observations.

As before, a significant drift was observed at negative radial velocities, as a rule, in VLA 2.

For example, an appreciable velocity drift from -10.5 to -12 km/s was detected in 2013–2014, at a drift rate of 0.1 km/s per month. This emission most likely arose in some fragment of the VLA 2 envelope, for example, in a filament or chain with a radial velocity gradient oriented radially with respect to the star. The shock produced during a flare sequentially propagates through the elements of such structures, exciting maser emission there. For a shock velocity of ~ 15 km/s, the filament length would be about 4 AU. This picture agrees with the results of VLA-observations [6, 7].

Figures 6 and 7 show the presence of flux-density variations for the main features. It is interesting to compare the evolutions of features belonging to the same configuration. The largest number of flaring features was associated with configuration 7.

The durations of flares at the 0.5 level were several months. During each flare associated with configuration 7, we observed a slight drift of the radial velocity, with the velocity always decreasing.

3.2. Line Shapes during Individual Flares

The width of a spectral line is described by the expression

$$V_D = \sqrt{V_{\text{th}}^2 + V_{\text{turb}}^2}, \quad (1)$$

where V_{th} is the thermal line width and V_{turb} is the turbulent line width. The line shape may be Gaussian and symmetric. However, under certain conditions the line may be asymmetric.

During strong flares the fluxes of individual features increase by more than a factor of ten. For single lines associated with an unsaturated maser, an increase in the flux density F is accompanied by narrowing of the line (ΔV):

$$\Delta V \propto (\ln F_0)^{-1/2}. \quad (2)$$

In the case of a saturated maser,

$$\Delta V \propto F_0^{-1/2}. \quad (3)$$

Here, F_0 is the flux at the line center.

This effect has been repeatedly observed in many sources (see, e.g., [21, 22]), and was associated with simple structures, such as homogeneous, spherical gas condensations. The observations we are considering here showed that all lines were only a factor of 1.5–2 narrower than during periods of low activity [19], even during their maximum emission. The formation of the line shape is strongly influenced by inhomogeneity of the medium and turbulent motions. When considering line formation, we must take into account the distributions of molecules along the lines of sight in all directions within the antenna beam. The fluxes in all these directions are added. Therefore, the emission intensity can substantially increase without appreciable narrowing of the line.

We did not detect any case when relationships (2) and (3) were satisfied. As at earlier observing epochs, the lines were wide during flares, with widths exceeding 0.8 km/s. This suggests an absence of maser features with simple structures. It is also possible that the physical parameters of the medium where the H_2O maser emission arises are variable [22].

Thus, analysis of the line shapes during flare maxima demonstrated an absence of the simplest structures—homogeneous maser condensations.

In the model for the maser sources (see, e.g., [19]), the temperature of the medium is typically taken to be 400 K. The corresponding thermal line width is 2.7 km/s. In contrast, the width of the narrowest line in our observations is about 1 km/s (Fig. 6). The observed increase in the intensity by a factor of ten requires an increase in the optical depth by a factor of four. This condition can easily be met with the high densities in maser condensations and in the presence of strong inhomogeneity of the medium.

Thus, the object VLA 1 (radio jet) is now in a stage of high activity, and has hosted a large number of powerful flares. The emission of configuration 7, which was the most stable configuration for many years, disappeared at the end of 2016. This region had earlier displayed the most intensive emission. However, the source activity did not decrease, its maximum only moved to another part of the spectrum. We suppose that the structure of the radio jet

changed, as occurred earlier, according to the 2012 observations [5].

3.3. Variability of the OH Maser Emission

Most of the main-line OH emission features demonstrated strong variability in both circular polarizations. Comparison with other observations performed before 2010 also shows the presence of high variability and flares in individual features. One can determine the predominant velocities of the main emission features in the spectra. A comparison of the spectra in the main lines shows only a partial coincidence in the velocities. The radial velocities of emission features did not change.

One exception was the 2015 flare at 1667 MHz. This feature was double, with component velocities at -5 and -4 km/s. We observed the flare on the ascending branch of its evolution. The radial velocity of the second component drifted by 0.4 km/s, while the velocity of the first component did not change.

Correlated variations were observed at 1667 MHz between the right-circularly polarized emission of the features at 10.0 and 12.5 km/s, as well as at -4.9 and -4.2 km/s.

The OH lines were fairly narrow; the widths of single lines were 0.21–0.26 km/s. However, most of the OH spectral features were superpositions of two to four narrower components. In these cases, we estimated the widths of the individual components using the right or left wings of the line. The results were similar: the widths were about 0.20–0.25 km/s. For a medium temperature of 60 K, the thermal line width is about 1 km/s. Hence, strong narrowing of the line as a result of maser amplification takes place.

3.4. Magnetic Fields in the Regions of OH Emission

During the strong flare in 2007–2009, Zeeman splitting was detected at 1667 MHz at a radial velocity of $V_{\text{LSR}} = 5.5$ km/s [23]. During our observations in 2010–2016 (our present study), the emission was weaker and was 100% circularly polarized. However, Zeeman splitting appeared at 1665 MHz at the same velocity as the one at which it was previously observed at 1667 MHz. The splitting was slightly less than at 1667 MHz, ~ 0.30 – 0.35 km/s. The corresponding magnetic field is 0.5–0.6 mG (see Fig. 9). We obtained this result for two features in this spectral region (at 5.4 and 5.7 km/s).

For most of the observed epochs, we were also able to measure the Zeeman splitting of weaker lines in this spectral region, which proved to be ~ 0.35 km/s. This splitting corresponds to a radial magnetic field

of ~ 0.6 mG. Thus, the magnetic-field strengths for three features with closely spaced radial velocities ~ 5.5 km/s all proved to be nearly the same. This additionally confirms that the maser features are formed by a compact cluster of maser spots, i.e., they are located in a strongly fragmented medium.

Magnetic fields of the order of a milliGauss could be created in this star-forming region as a result of compression of the circumstellar gas by the wind from a young star (for example, by a MHD wave). The strong flares of the OH maser and rapid variability of the emission could also be related to compression at such a shock front.

The absence of VLBI observations hindered the direct detection of widely separated Zeeman pairs, as was done, for example, in [16].

4. CONCLUSION

We have studied strong flares of the H₂O maser emission in W75 N occurring in 2011–2017.

A large number of strong flares with amplitudes exceeding 1000 Jy occurred during this time interval. The flare emission was mostly identified with the radio jet associated with VLA 1. This emission was observed in a narrow range of radial velocities (9.5–11.5 km/s), and the line shapes changed significantly in the course of its evolution. We detected the sequential excitation of maser features with closely spaced radial velocities, formed by clusters of maser features. Time delays varied from two to seven months, which corresponds to maser-cluster sizes of up to 1.8 AU, for a shock velocity of 15 km/s. Differences in the time delays for different epochs could be related to the existence of turbulence and proper motions of the maser features that change the structures of the maser clusters.

Our study of the line shapes during flare maxima has demonstrated an absence of the simplest structures, such as homogeneous maser condensations.

We also identified emission at radial velocities from -10.5 to -12 km/s, displaying a drift rate of 0.1 km/s per month. This emission is associated with an extended structure (possibly a filament) about 4 AU long, located in the envelope of the VLA 2 disk.

We observed a strong variability of individual OH maser features at 1665 and 1667 MHz. Three features belonging to the same maser cluster demonstrated Zeeman splittings at 1665 MHz corresponding to a radial magnetic field of about 0.5 mG. The inferred magnetic field varies in the range 0.4–0.6 mG.

The line widths of individual features were about 0.20–0.25 km/s; this is a factor of four to five narrower than the thermal line width, indicating the existence of strong maser effects. The flares of the OH

masers and the rapid variability of their emission may be related to compression at the front of an MHD wave.

ACKNOWLEDGMENTS

This work was supported by the Russian Foundation for Basic Research (project 15-02-07676). We are grateful to the staff of the Meudon (France) and Pushchino (Russia) Radio Astronomy Observatories for help during the observations.

REFERENCES

1. J. M. Torrelles, J. F. Gómez, L. F. Rodríguez, P. T. P. Ho, S. Curiel, and R. Vázquez, *Astrophys. J.* **489**, 744 (1997).
2. C. G. Wynn-Williams, E. E. Becklin, and G. Neugebauer, *Astrophys. J.* **187**, 473 (1974).
3. A. D. Haschick, M. J. Reid, B. F. Burke, J. M. Moran, and G. Miller, *Astrophys. J.* **244**, 76 (1981).
4. G. Surcis, W. H. T. Vlemmings, and H. Dodson, *Astron. Astrophys.* **506**, 757 (2009).
5. G. Surcis, W. H. T. Vlemmings, H. J. van Langevelde, C. Goddi, J. M. Torrelles, J. Cantó, S. Curiel, S.-W. Kim, and J.-S. Kim, *Astron. Astrophys.* **565**, L8 (2014).
6. J. M. Torrelles, L. A. Patel, G. Anglada, J. F. Gómez, P. T. P. Ho, L. Lara, A. Alberdi, J. Cantó, S. Curiel, G. Garay, and L. F. Rodríguez, *Astrophys. J.* **598**, L115 (2003).
7. E. E. Lekht, V. I. Slysh, and V. V. Krasnov, *Astron. Rep.* **51**, 967 (2007).
8. E. E. Lekht, V. I. Slysh, and V. V. Krasnov, *Astron. Rep.* **53**, 420 (2009).
9. M. Szymczak and E. Gérard, *Astron. Astrophys.* **494**, 117 (2009).
10. W. T. Sullivan III and J. H. Kerstholt, *Astron. Astrophys. Suppl. Ser.* **26**, 399 (1976).
11. A. V. Alakoz, V. I. Slysh, M. V. Popov, and I. E. Val'tts, *Astron. Lett.* **31**, 375 (2005).
12. A. L. Argon, M. J. Reid, and K. M. Menten, *Astrophys. J. Suppl.* **129**, 159 (2000).
13. V. L. Fish, M. Gray, W. M. Goss, and A. M. S. Richards, *Mon. Not. R. Astron. Soc.* **417**, 555 (2011).
14. V. I. Slysh, V. Migenes, I. E. Val'tts, S. Yu. Lyubchenko, S. Horiuchi, V. I. Altunin, E. B. Fomalont, and M. Inoue, *Astrophys. J.* **564**, 317 (2002).
15. B. Hutawarakorn, R. J. Cohen, and G. C. Brebner, *Mon. Not. R. Astron. Soc.* **330**, 349 (2002).
16. V. I. Slysh and V. Migenes, *Mon. Not. R. Astron. Soc.* **369**, 1497 (2006).
17. E. E. Lekht and R. L. Sorochenko, *Sov. Astron. Lett.* **10**, 307 (1984).
18. E. E. Lekht and V. V. Krasnov, *Astron. Lett.* **26**, 38 (2000).
19. G. Surcis, W. H. T. Vlemmings, S. Curiel, B. Hutawarakorn Kramer, J. M. Torrelles, and A. P. Sarma, *Astron. Astrophys.* **527**, A48 (2011).
20. J.-S. Kim, S.-W. Kim, T. Kurayama, M. Honma, T. Sasao, G. Surcis, J. Cantó, J. M. Torrelles, and S.-J. Kim, *Astrophys. J.* **767**, 86 (2013).
21. L. I. Matveenko, P. H. Diamond, and D. A. Graham, *Astron. Rep.* **44**, 592 (2000).
22. E. E. Lekht, *Astron. Astrophys. Suppl. Ser.* **141**, 185 (2000).
23. V. I. Slysh, M. I. Pashchenko, G. M. Rudnitskii, V. M. Vitrishchak, and P. Colom, *Astron. Rep.* **54**, 599 (2010).

Translated by S. Kalenskii